

Strong gravitational lensing by Kerr and Kerr-Newman black holes

Tien Hsieh, Da-Shin Lee,^{*} and Chi-Yong Lin[†]

*Department of Physics, National Dong Hwa University,
Hualien 97401, Taiwan, Republic of China*

(Dated: March 1, 2022)

Abstract

We study the strong gravitational lensing due to the Kerr black holes with angular momentum a and the Kerr-Newman black holes with additional charge Q . We first derive the analytical expressions of the deflection angles of light rays that particularly diverge as they travel near the photon sphere. In this strong deflection limit, the light rays can circle around the black hole multiple times before reaching the observer, giving relativistic images. The obtained analytical expressions are then applied to compute the angular positions of relativistic images due to the supermassive galactic black holes. In this work, we focus on the outermost image with reference to the optical axis. We find that its angular separation from the one closest to the optical axis increases with the increase of angular momentum a of the black holes for light rays in direct orbits. Additionally, the effects of the charge Q of black holes also increase the angular separation of the outermost image from the others for both direct and retrograde orbits. The potentially increasing observability of the relativistic images from the effects of angular momentum and charge of the black holes will be discussed.

PACS numbers: 04.70.-s, 04.70.Bw, 04.80.Cc

^{*}Electronic address: dslee@gms.ndhu.edu.tw

[†]Electronic address: lyong@gms.ndhu.edu.tw

I. INTRODUCTION

Gravitational lensing is one of the powerful tools to test general relativity (GR) [1, 2]. Weak lensing has been fully studied in the formalism of weak field approximations, which can be used to successfully explain various lensing phenomena in a broad array of astrophysical contexts [3]. Nevertheless, in recent years, there have been significant theoretical studies looking into lensing phenomena from strong field perspectives [4–15]. Through the gravitational lensing in the vicinity of the compact massive objects such as a black hole would provide another avenue to test GR. So far, observational evidence has shown that almost every large galaxy has a supermassive black hole at the galaxy’s center [16]. The Milky Way has a supermassive black hole in its Galactic Center with the location of Sagittarius A* [17, 18]. Together with the first image of the black hole captured by the Event Horizon Telescope [19–21], gravitational lensing will also become an important probe to study the isolated dim black hole.

Recently, Virbhadra and Ellis have developed a new gravitational lens equation, which allows us to study large deflection of light rays, resulting in the strong gravitational lensing [4]. This lens equation is then applied to analyze the lensing by a Schwarzschild black hole in the center of the galaxy using numerical methods. Later, Frittelli *et al.* propose the definition of an exact lens equation without reference to the background spacetime, and construct the exact lens equation explicitly in the Schwarzschild spacetime [5]. Strong field lensing in the general spherically symmetric and static spacetime is first studied analytically by Bozza in [6, 7, 9] and later by Tsukamoto in [12, 13]. These works show that the deflection angle $\hat{\alpha}(b)$ of light rays for a given impact parameter b , which in the strong deflection limit (SDL) as $b \rightarrow b_c$, can be approximated in the form

$$\hat{\alpha}(b) \approx -\bar{a} \log \left(\frac{b}{b_c} - 1 \right) + \bar{b} + O((b - b_c) \log(b - b_c)) \quad (1)$$

with two parameters \bar{a} and \bar{b} as a function of the black hole’s parameters. Then, in [8], the Kerr black hole of the nonspherically symmetric black holes is considered, exploring \bar{a} and \bar{b} numerically. In this paper, we extend the works of [6] and [12, 13] and find the analytic form of \bar{a} and \bar{b} for nonspherically symmetric Kerr and Kerr-Newman black holes, respectively, using the analytical closed-form expressions of the deflection angles in [22] and [23]. Although one might not expect that astrophysical black holes have large residue electric

charge, some accretion scenarios are proposed to investigate the possibility of the spinning charged black holes [24, 25]. It is then still of great interest to extend the studies to the Kerr-Newman black holes [26–28]. The analytical expressions can be applied to examine the lensing effects due to the supermassive galactic black holes as illustrated in Fig.(1). The light rays are emitted from the source, and circle around the black hole multiple times in the SDL along a direct orbit (red line) or a retrograde orbit (blue line), giving two sets of the relativistic images. Following the approach of [7] enables us to study the observational consequences.

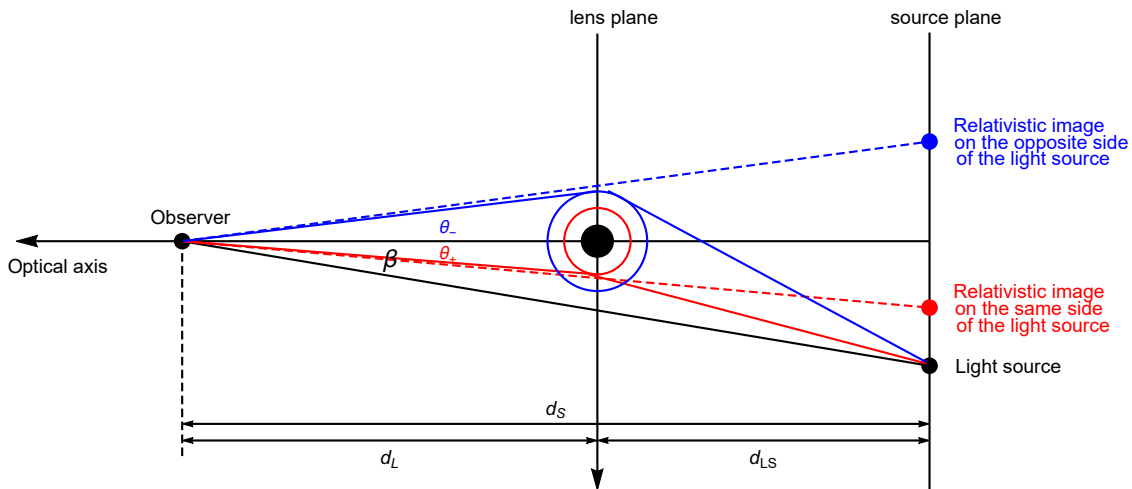


FIG. 1: Gravitational lens about relativistic images. Considering the Kerr or the Kerr-Newman black hole with angular momentum of the clockwise rotation, the light rays are emitted from the source, and circle around the black hole multiple times in the SDL along a direct orbit (red line) or a retrograde orbit (blue line). The graph illustrates two sets of the relativistic images.

The layout of the paper is as follows. In Sec.II, we first review the closed-form expression of the deflection angle due to the Kerr and/or the Kerr-Newman black holes. In particular, we discuss the results of the radius of the innermost circular motion of light rays as well as the associated critical impact parameters as a function of the black hole's parameters. These will serve as the important inputs to find the values of the coefficients \bar{a} and \bar{b} in the SDL deflection angle. Then we derive the analytic form of \bar{a} and \bar{b} in the cases of Kerr and Kerr-Newman black holes, respectively, and check the consistency with the known results from taking the proper limits of the black holes's parameters. In Sec. III, the analytical

expressions on the equatorial gravitational lensing are then applied to compute the angular positions of relativistic images due to the supermassive galactic black holes. When the light rays travel on the quasiequatorial plane, the obtained results for $\theta = \frac{\pi}{2}$ can also be used to estimate the magnification of relativistic images, as the light sources are near one of the caustic points with the additional inputs from the dynamics of the light rays in the angle θ . The potentially increasing observability of the relativistic images from the effects of angular momentum and charge of the black holes will be summarized in the closing section.

II. DEFLECTION ANGLE DUE TO BLACK HOLES IN THE STRONG DEFLECTION LIMIT

We consider nonspherically symmetric spacetimes of the Kerr and Kerr-Newman metrics respectively to obtain the deflection angle $\hat{\alpha}(b)$ of light rays for a given impact parameter b . In the SDL, as $b \rightarrow b_c$, $\hat{\alpha}(b)$ can be approximated in the form of (1). In what follows, we will consider the above two types of the black holes separately.

A. Kerr black holes

The line element of the Kerr black hole in which spacetime outside a black hole with the gravitational mass M and angular momentum per unit mass $a = J/M$ is described by

$$\begin{aligned} ds^2 &= g_{\mu\nu} dx^\mu dx^\nu \\ &= -\frac{(\Delta - a^2 \sin^2 \theta)}{\Sigma} dt^2 - \frac{a \sin^2 \theta (2Mr)}{\Sigma} (dt d\phi + d\phi dt) \\ &\quad + \frac{\Sigma}{\Delta} dr^2 + \Sigma d\theta^2 + \frac{\sin^2 \theta}{\Sigma} ((r^2 + a^2)^2 - a^2 \Delta \sin^2 \theta) d\phi^2 \end{aligned} \quad (2)$$

with

$$\Sigma = r^2 + a^2 \cos^2 \theta, \quad \Delta = r^2 + a^2 - 2Mr. \quad (3)$$

The outer (inner) event horizon r_+ (r_-) can be found by solving $\Delta(r) = 0$, and is given by

$$r_{\pm} = M \pm \sqrt{M^2 - a^2} \quad (4)$$

with the condition $M^2 > a^2$. Notice that we just adopt the notation of r_- where the light rays traveling outside the horizon are considered.

The Lagrangian of a particle is then

$$\mathcal{L} = \frac{1}{2} g_{\mu\nu} u^\mu u^\nu \quad (5)$$

with the 4-velocity $u^\mu = dx^\mu/d\lambda$ defined in terms of an affine parameter λ . The metric of the Kerr black hole, which is independent on t and ϕ , gives the associated Killing vectors $\xi_{(t)}^\mu$ and $\xi_{(\phi)}^\mu$

$$\xi_{(t)}^\mu = \delta_t^\mu, \quad \xi_{(\phi)}^\mu = \delta_\phi^\mu. \quad (6)$$

Then, together with 4-velocity of light rays, the conserved quantities along a geodesic, can be constructed by the above Killing vectors $\varepsilon \equiv -\xi_{(t)}^\mu u_\mu$ and $\ell \equiv \xi_{(\phi)}^\mu u_\mu$, where ε and ℓ are the light ray's energy and azimuthal angular momentum at spatial infinity. Light rays traveling along null world lines obey the condition $u^\mu u_\mu = 0$. To indicate whether the light rays are traversing along the direction of frame dragging or opposite to it, we define the following impact parameter :

$$b_s = s \left| \frac{\ell}{\varepsilon} \right| \equiv s b, \quad (7)$$

where $s = \text{Sign}(\ell/\varepsilon)$ and b is the positive magnitude. The parameter $s = +1$ for $b_s > 0$ will be referred to as direct orbits, and those with $s = -1$ for $b_s < 0$ as retrograde orbits (see Fig.(1) for the sign convention). Here we restrict the light rays traveling on the equatorial plane of the black hole by choosing $\theta = \pi/2$, and $\dot{\theta} = 0$. The equation of motion along the radial direction can be cast in the form [23]

$$\frac{1}{b^2} = \frac{\dot{r}^2}{\ell^2} + W_{\text{eff}}(r), \quad (8)$$

from which we define the function W_{eff} as

$$W_{\text{eff}}(r) = \frac{1}{r^2} \left[1 - \frac{a^2}{b^2} - \frac{2M}{r} \left(1 - \frac{a}{b_s} \right)^2 \right]. \quad (9)$$

The above equation is analogous to that of particle motion in the effective potential $W_{\text{eff}}(r)$ with the kinetic energy \dot{r}^2/ℓ^2 and constant total energy $1/b^2$. Let us consider that a light ray starts in the asymptotic region to approach the black hole, and then turns back to the asymptotic region to reach the observer. Such light rays have a turning point, the closest approach distance to a black hole r_0 , which crucially depends on the impact parameter b ,

determined by

$$\left. \frac{\dot{r}^2}{\ell^2} \right|_{r=r_0} = \frac{1}{b^2} - W_{\text{eff}}(r_0) = 0. \quad (10)$$

From (10), also shown in [22, 23], one can find the impact parameter b for a given r_0 , which becomes the important input for the analytical expressions of the deflection angle in the SDL, as

$$b(r_0) = \frac{2sMa - r_0\sqrt{a^2 - 2r_0M + r_0^2}}{2M - r_0}. \quad (11)$$

The behavior of the light ray trajectories depends on whether $1/b^2$ is greater or less than the maximum height of $W_{\text{eff}}(r)$. The innermost trajectories of light rays have a direct consequence on the apparent shape of the black hole. The smallest radius r_{sc} , when the turning point r_0 is located at the maximum of $W_{\text{eff}}(r)$, with the critical impact parameter b_{sc} , obeys

$$\left. \frac{dW_{\text{eff}}(r)}{dr} \right|_{r=r_{sc}} = 0. \quad (12)$$

Then the radius of the circular motion forming the photon sphere is given by (See [22, 23]).

$$r_{sc} = 2M \left\{ 1 + \cos \left[\frac{2}{3} \cos^{-1} \left(\frac{-sa}{M} \right) \right] \right\} \quad (13)$$

with the corresponding impact parameter

$$b_{sc} = -a + s6M \cos \left[\frac{1}{3} \cos^{-1} \left(\frac{-sa}{M} \right) \right]. \quad (14)$$

In the case of a Kerr black hole, the nonzero spin of the black hole is found to give more repulsive effects to the light rays in the direct orbits than those in the retrograde orbits due to the $1/r^3$ term in the effective potential. The repulsive effects in turn affect light rays in the direct orbits in a way to prevent them from collapsing into the event horizon. As a result, this shifts the innermost circular trajectories of the light rays toward the black hole with the smaller critical impact parameter b_{+c} than b_{-c} in the retrograde orbits as shown in Fig.(2). As such, when a increases, the impact parameter b_{+c} decreases whereas $|b_{-c}|$ increases instead [22, 23]. It will be shown in the next section that the value of b_{sc} is a key quantity to determine the features of the angular position of the induced images of the distant light sources due to the strong gravitational lensing effects. Also, the presence of black hole's spin is to give the smaller deflection angle in the direct orbits as compared with the retrograde orbits with the same impact parameter b [22, 23].

We proceed by introducing the variable

$$z \equiv 1 - \frac{r_0}{r} . \quad (15)$$

The geodesic equations for r and ϕ found in [23] can be rewritten in terms of z as [12]

$$\frac{dz}{d\phi} = \frac{1}{r_0} \frac{1 - \frac{2M}{r_0}(1-z) + \frac{a^2}{r_0^2}(1-z)^2}{1 - \frac{2M}{r_0}(1-z)(1 - \frac{a}{b_s})} \sqrt{B(z, r_0)} , \quad (16)$$

where the function $B(z, r_0)$ has the trinomial form in z

$$B(z, r_0) = c_1(r_0)z + c_2(r_0)z^2 + c_3(r_0)z^3 \quad (17)$$

with the coefficients

$$\begin{aligned} c_1(r_0) &= -6Mr_0 \left(1 - \frac{a}{b_s}\right)^2 + 2r_0^2 \left(1 - \frac{a^2}{b^2}\right) , \\ c_2(r_0) &= 6Mr_0 \left(1 - \frac{a}{b_s}\right)^2 - r_0^2 \left(1 - \frac{a^2}{b^2}\right) , \\ c_3(r_0) &= -2Mr_0 \left(1 - \frac{a}{b_s}\right)^2 . \end{aligned} \quad (18)$$

Next we rewrite

$$\frac{1 - \frac{2M}{r_0}(1 - \frac{a}{b_s}) + \frac{2M}{r_0}(1 - \frac{a}{b_s})z}{1 - \frac{2M}{r_0} + \frac{a^2}{r_0^2} + (\frac{2M}{r_0} - \frac{2a^2}{r_0^2})z + \frac{a^2}{r_0^2}z^2} = \frac{r_0^2}{a^2} \left(\frac{C_-}{z - z_-} + \frac{C_+}{z - z_+} \right) , \quad (19)$$

where the roots z_- , z_+ , and the coefficients C_- , C_+ are

$$\begin{aligned} z_- &= 1 - \frac{r_0 r_-}{a^2} , \\ z_+ &= 1 - \frac{r_0 r_+}{a^2} , \\ C_- &= \frac{a^2 - 2Mr_-(1 - \frac{a}{b_s})}{2r_0 \sqrt{M^2 - a^2}} , \\ C_+ &= \frac{-a^2 + 2Mr_+(1 - \frac{a}{b_s})}{2r_0 \sqrt{M^2 - a^2}} \end{aligned} \quad (21)$$

with r_+ (r_-) being the outer (inner) horizon of a Kerr black hole defined in (4). Also note that z_- , $z_+ \leq 0$, for all spin a . Then the deflection angle can be calculated as a function of the closest approach distance r_0 from (16) giving

$$\hat{\alpha}(r_0) = I(r_0) - \pi , \quad I(r_0) = \int_0^1 f(z, r_0) dz , \quad (22)$$

where the integrand becomes

$$f(z, r_0) = \frac{r_0^2}{a^2} \left(\frac{C_-}{z - z_-} + \frac{C_+}{z - z_+} \right) \frac{2r_0}{\sqrt{c_1(r_0)z + c_2(r_0)z^2 + c_3(r_0)z^3}}. \quad (23)$$

In the SDL of our interest, when the closest approach distance reaches its critical limit, namely $r_0 \rightarrow r_{sc}$, and $c_1(r_0) \rightarrow 0$ in (18) obtained from (12), the integrand $f(z, r_0) \rightarrow \frac{1}{z}$ for small z leads to the logarithmic divergence as $r_0 \rightarrow r_{sc}$. Let us now define a new function $f_D(z, r_0)$

$$f_D(z, r_0) = \frac{r_0^2}{a^2} \left(\frac{C_-}{z - z_-} + \frac{C_+}{z - z_+} \right) \frac{2r_0}{\sqrt{c_1(r_0)z + c_2(r_0)z^2}}, \quad (24)$$

that separates the divergent part from the regular part given by $f_R(z, r_0) = f(z, r_0) - f_D(z, r_0)$. The integral of f_R is thus finite.

The divergent part comes from an integral of the function $f_D(z, r_0)$, which contributes not only to \bar{a} for the logarithmic term but also \bar{b} for the regular part in (1), giving

$$\begin{aligned} I_D(r_0) &= \int_0^1 f_D(z, r_0) dz \\ &= \frac{2r_0^3}{a^2} \frac{C_-}{\sqrt{c_1(r_0)z_- + c_2(r_0)z_-^2}} \log \left(\frac{\sqrt{c_1(r_0)z_- + c_2(r_0)z_-} + \sqrt{c_1(r_0) + c_2(r_0)z_-}}{\sqrt{c_1(r_0)z_- + c_2(r_0)z_-} - \sqrt{c_1(r_0) + c_2(r_0)z_-}} \right) \\ &\quad + \frac{2r_0^3}{a^2} \frac{C_+}{\sqrt{c_1(r_0)z_+ + c_2(r_0)z_+^2}} \log \left(\frac{\sqrt{c_1(r_0)z_+ + c_2(r_0)z_+} + \sqrt{c_1(r_0) + c_2(r_0)z_+}}{\sqrt{c_1(r_0)z_+ + c_2(r_0)z_+} - \sqrt{c_1(r_0) + c_2(r_0)z_+}} \right). \end{aligned} \quad (25)$$

In the SDL, the expansions of the coefficient $c_1(r_0)$ (18) and the impact parameter $b(r_0)$ in powers of small $r_0 - r_{sc}$ read

$$c_1(r_0) = c'_{1sc}(r_0 - r_{sc}) + O(r_0 - r_{sc})^2, \quad (26)$$

$$b(r_0) = b_{sc} + \frac{b''_{sc}}{2!}(r_0 - r_{sc})^2 + O(r_0 - r_{sc})^3, \quad (27)$$

where $c_1(r_{sc}) \equiv c_{1sc} = 0$ and $b(r_{sc}) \equiv b_{sc}$ is the critical impact parameter given by (14). The subscript sc denotes evaluating the function at $r = r_{sc}$. The prime means the derivative with respect to r_0 . Notice that using $c_{1sc} = 0$ in (18), one finds

$$c_{3sc} = -\frac{2}{3}c_{2sc}. \quad (28)$$

Combining (26) with (27), we can write $c_1(r_0)$ in terms of small $b - b_{sc}$ as

$$\lim_{r_0 \rightarrow r_{sc}} c_1(r_0) = \lim_{b \rightarrow b_{sc}} c'_{1sc} \sqrt{\frac{2b_{sc}}{b''_{sc}}} \left(\frac{b}{b_{sc}} - 1 \right)^{1/2}. \quad (29)$$

In the SDL, substituting (29) into (25), I_D becomes

$$I_D(b) \simeq - \left(\frac{r_{sc}^3}{a^2} \frac{C_{-sc}}{\sqrt{c_{2sc} z_{-sc}^2}} + \frac{r_{sc}^3}{a^2} \frac{C_{+sc}}{\sqrt{c_{2sc} z_{+sc}^2}} \right) \log \left(\frac{b}{b_{sc}} - 1 \right) \\ + \frac{r_{sc}^3}{a^2} \frac{C_{-sc}}{\sqrt{c_{2sc} z_{-sc}^2}} \log \left(\frac{16 c_{2sc}^2 z_{-sc}^2 b_{sc}''}{c_{1sc}^2 2b_{sc} (z_{-sc} - 1)^2} \right) + \frac{r_{sc}^3}{a^2} \frac{C_{+sc}}{\sqrt{c_{2sc} z_{+sc}^2}} \log \left(\frac{16 c_{2sc}^2 z_{+sc}^2 b_{sc}''}{c_{1sc}^2 2b_{sc} (z_{+sc} - 1)^2} \right). \quad (30)$$

Finally, the coefficients \bar{a} and the contribution from $I_D(b)$ to \bar{b} denoted by b_D in (1) are

$$\bar{a} = \frac{r_{sc}^3}{\sqrt{c_{2sc}}} \left[\frac{C_{-sc}}{r_{sc} r_- - a^2} + \frac{C_{+sc}}{r_{sc} r_+ - a^2} \right] \quad (31)$$

and

$$b_D = \bar{a} \log \left[\frac{8c_{2sc}^2 b_{sc}''}{c_{1sc}^2 b_{sc}} \right] + \frac{2r_{sc}^3}{\sqrt{c_{2sc}}} \left[\frac{C_{-sc}}{r_{sc} r_- - a^2} \log \left(1 - \frac{a^2}{r_{sc} r_-} \right) + \frac{C_{+sc}}{r_{sc} r_+ - a^2} \log \left(1 - \frac{a^2}{r_{sc} r_+} \right) \right], \quad (32)$$

where z_{\pm} are replaced by r_{\pm} through (20). The leading order result in the SDL from the integration of $f_R(z, r_{sc})$, which contributes the coefficient \bar{b} , is denoted by b_R , and is obtained as

$$b_R = I_R(r_{sc}) = \int_0^1 f_R(z, r_{sc}) dz \\ = \frac{2r_0^3}{a^2} \frac{C_-}{\sqrt{c_2 z_-}} \log \left(\frac{z_-}{z_- - 1} \frac{\sqrt{c_2 + c_3} + \sqrt{c_2}}{\sqrt{c_2 + c_3} - \sqrt{c_2}} \frac{c_3}{4c_2} \right) \\ + \frac{2r_0^3}{a^2} \frac{C_-}{\sqrt{c_2 + c_3 z_- z_-}} \log \left(\frac{\sqrt{c_2 + c_3 z_-} - \sqrt{c_2 + c_3}}{\sqrt{c_2 + c_3 z_-} + \sqrt{c_2 + c_3}} \frac{\sqrt{c_2 + c_3 z_-} + \sqrt{c_2}}{\sqrt{c_2 + c_3 z_-} - \sqrt{c_2}} \right) \\ + \frac{2r_0^3}{a^2} \frac{C_+}{\sqrt{c_2 z_+}} \log \left(\frac{z_+}{z_+ - 1} \frac{\sqrt{c_2 + c_3} + \sqrt{c_2}}{\sqrt{c_2 + c_3} - \sqrt{c_2}} \frac{c_3}{4c_2} \right) \\ + \frac{2r_0^3}{a^2} \frac{C_+}{\sqrt{c_2 + c_3 z_+ z_+}} \log \left(\frac{\sqrt{c_2 + c_3 z_+} - \sqrt{c_2 + c_3}}{\sqrt{c_2 + c_3 z_+} + \sqrt{c_2 + c_3}} \frac{\sqrt{c_2 + c_3 z_+} + \sqrt{c_2}}{\sqrt{c_2 + c_3 z_+} - \sqrt{c_2}} \right) \Big|_{r_0=r_{sc}}. \quad (33)$$

Thus, the coefficient \bar{b} can be computed from the sum of b_D and b_R

$$\bar{b} = -\pi + b_D + b_R \quad (34)$$

with the help of (32) and (33). In (33) we again use (28) and (20) to replace c_{3sc} by

$c_{2sc} = -\frac{2}{3}c_{3sc}$ and z_{\pm} by r_{\pm} . After some straightforward algebra we find

$$\begin{aligned} \bar{b} = & -\pi + \bar{a} \log \left(\frac{36}{7+4\sqrt{3}} \frac{8c_{2sc}^2 b_{sc}''}{c_{1sc}^2 b_{sc}} \right) \\ & + \frac{r_{sc}^3}{\sqrt{c_{2sc}}} \frac{2aC_{-sc}}{a^2 - r_{sc}r_-} \frac{\sqrt{3}}{\sqrt{a^2 + 2r_{sc}r_-}} \log \left(\frac{\sqrt{a^2 + 2r_{sc}r_-} - a}{\sqrt{a^2 + 2r_{sc}r_-} + a} \frac{\sqrt{a^2 + 2r_{sc}r_-} + \sqrt{3}a}{\sqrt{a^2 + 2r_{sc}r_-} - \sqrt{3}a} \right) \\ & + \frac{r_{sc}^3}{\sqrt{c_{2sc}}} \frac{2aC_{+sc}}{a^2 - r_{sc}r_+} \frac{\sqrt{3}}{\sqrt{a^2 + 2r_{sc}r_+}} \log \left(\frac{\sqrt{a^2 + 2r_{sc}r_+} - a}{\sqrt{a^2 + 2r_{sc}r_+} + a} \frac{\sqrt{a^2 + 2r_{sc}r_+} + \sqrt{3}a}{\sqrt{a^2 + 2r_{sc}r_+} - \sqrt{3}a} \right). \end{aligned} \quad (35)$$

Using the results of r_{sc} (13), b_{sc} (14) and the expression of $b(r_0)$ (11), together with the definitions of C_{\pm} and c_2 in (21) and (18) respectively, one can compute the coefficients \bar{a} and \bar{b} given by (31) and (35) in the form of (1). Notice that with the parameters under investigation $\bar{a} > 0$, but $\bar{b} < 0$. Our results are shown in Fig.(3), where both \bar{a} and $|\bar{b}|$ increase (decrease) in a in direct (retrograde) orbits, giving the fact that the deflection angle $\hat{\alpha}$ decreases (increases) with the increase of the black hole's spin for a given impact parameter. Later in Sec. III we will compare with the full numerical computations from (22) in the SDL.

The results of \bar{a} and \bar{b} due to the Schwarzschild black hole in [7, 12] can be reproduced by sending $a \rightarrow 0$ where $r_+ \rightarrow 2M$, $r_- \rightarrow a^2/2M$, $C_{+sc} \rightarrow 2M/r_{sc}$, $C_{-sc} \rightarrow a^3/2b_{sc}Mr_{sc}$, and $c_{2sc} \rightarrow r_{sc}^2$ using $c_{1sc} = 0$ in (4) and (21). We can check that $\bar{a} = 1$ in (31) and \bar{b} in (35) reduces to the expression proportional to \bar{a} given by

$$\begin{aligned} \bar{b} = & -\pi + \bar{a} \log \left(36(7-4\sqrt{3}) \frac{8c_{2sc}^2 b_{sc}''}{c_{1sc}^2 b_{sc}} \right) \\ = & -\pi + \log \left(216(7-4\sqrt{3}) \right). \end{aligned} \quad (36)$$

In the second equality above we have further used substitutions $b_{sc} \rightarrow 3\sqrt{3}M$, $b_{sc}'' \rightarrow \sqrt{3}/M$, $c_{1sc}' \rightarrow 6M$, and $c_{2sc} \rightarrow 9M^2$ obtained from $r_{sc} = 3M$ in the Schwarzschild black hole. In Fig.(5), we compare the approximate results of the deflection angle in the SDL with the exact ones in [22] and [23], and find that they are in good agreement when $b \rightarrow b_{sc}$.

The analytical expressions of the coefficient \bar{a} and \bar{b} in the form of the SDL deflection angle due to the Kerr black hole are successfully achieved. They are an extension of the works in [9] and [12] where the spherically symmetric black holes are considered. This is one of the main results in this work.

B. Kerr-Newman black holes

We now consider another example with the nonspherically symmetric metric of a charged spinning black hole. With an addition of charge Q comparing with the Kerr case, the line element associated with the Kerr-Newman metric is

$$\begin{aligned} ds^2 &= g_{\mu\nu} dx^\mu dx^\nu \\ &= -\frac{(\Delta - a^2 \sin^2 \theta)}{\Sigma} dt^2 + \frac{a \sin^2 \theta (Q^2 - 2Mr)}{\Sigma} (dt d\phi + d\phi dt) \\ &\quad + \frac{\Sigma}{\Delta} dr^2 + \Sigma d\theta^2 + \frac{\sin^2 \theta}{\Sigma} ((r^2 + a^2)^2 - a^2 \Delta \sin^2 \theta) d\phi^2, \end{aligned} \quad (37)$$

where

$$\Sigma = r^2 + a^2 \cos^2 \theta, \quad \Delta = r^2 + a^2 + Q^2 - 2Mr. \quad (38)$$

The outer (inner) event horizon r_+ (r_-) is

$$r_{\pm} = M \pm \sqrt{M^2 - (Q^2 + a^2)} \quad (39)$$

with $M^2 > Q^2 + a^2$.

The light rays traveling on the equatorial plane of the black hole have been studied analytically in our previous work in [23], in which the function W_{eff} from the equation of motion along the radial direction in (8) can be regarded as an effective potential given by

$$W_{\text{eff}}(r) = \frac{1}{r^2} \left[1 - \frac{a^2}{b^2} + \left(-\frac{2M}{r} + \frac{Q^2}{r^2} \right) \left(1 - \frac{a}{b_s} \right)^2 \right]. \quad (40)$$

For the Kerr-Newman black hole, the nonzero charge of the black hole is found to give repulsive effects to light rays as seen from its contributions to the function W_{eff} of the $1/r^4$ term, which shifts the innermost circular trajectories of the light rays toward the black holes with the smaller critical impact parameter b_{sc} for both direct and retrograde orbits, as illustrated in Fig.(2). Also, the presence of black hole's charge is to decrease the deflection angle due to the additional repulsive effects on the light rays, as compared with the Kerr case with the same impact parameter b [23]. As we will discuss in the next section, the angular positions of the relativistic images of the distant light sources due to the gravitational lensing of the black holes critically depends on the critical impact parameter b_{sc} .

The impact parameter b as a function of the radius of the circular motion r_0 is obtained

as

$$b(r_0) = \frac{s(2aM - a\frac{Q^2}{r_0}) - r_0\sqrt{(a\frac{Q^2}{r_0^2} - a\frac{2M}{r_0})^2 + (1 - \frac{2M}{r_0} + \frac{Q^2}{r_0^2})[a^2(1 + \frac{2M}{r_0} - \frac{Q^2}{r_0^2}) + r_0^2]}}{2M - r_0 - \frac{Q^2}{r_0}}. \quad (41)$$

The solution of r_{sc} of the radius of the innermost circular motion has been found in [23] as

$$r_{sc} = \frac{3M}{2} + \frac{1}{2\sqrt{3}}\sqrt{9M^2 - 8Q^2 + U_c + \frac{P_c}{U_c}} - \frac{s}{2}\sqrt{6M^2 - \frac{16Q^2}{3} - \frac{1}{3}\left(U_c + \frac{P_c}{U_c}\right) + \frac{8\sqrt{3}Ma^2}{\sqrt{9M^2 - 8Q^2 + U_c + \frac{P_c}{U_c}}}}, \quad (42)$$

where

$$P_c = (9M^2 - 8Q^2)^2 - 24a^2(3M^2 - 2Q^2),$$

$$U_c = \left\{ (9M^2 - 8Q^2)^3 - 36a^2(9M^2 - 8Q^2)(3M^2 - 2Q^2) + 216M^2a^4 + 24\sqrt{3}a^2\sqrt{(M^2 - a^2 - Q^2)[Q^2(9M^2 - 8Q^2)^2 - 27M^4a^2]} \right\}^{\frac{1}{3}}. \quad (43)$$

The analytical expression of the critical value of the impact parameter b_{sc} can be written as a function of black hole's parameters [23],

$$b_{sc} = -a + \frac{M^2a}{2(M^2 - Q^2)} + \frac{s}{2\sqrt{3}(M^2 - Q^2)} \left[\sqrt{V + (M^2 - Q^2)\left(U + \frac{P}{U}\right)} + \sqrt{2V - (M^2 - Q^2)\left(U + \frac{P}{U}\right) - \frac{s6\sqrt{3}M^2a[(M^2 - Q^2)(9M^2 - 8Q^2)^2 - M^4a^2]}{\sqrt{V + (M^2 - Q^2)\left(U + \frac{P}{U}\right)}}} \right], \quad (44)$$

where

$$P = (3M^2 - 4Q^2)[9(3M^2 - 4Q^2)^3 + 8Q^2(9M^2 - 8Q^2)^2 - 216M^4a^2],$$

$$U = \left\{ -[3(3M^2 - 2Q^2)^2 - 4Q^4][9M^2(9M^2 - 8Q^2)^3 - 8[3(3M^2 - 2Q^2)^2 - 4Q^4]^2] + 108M^4a^2[9(3M^2 - 4Q^2)^3 + 4Q^2(9M^2 - 8Q^2)^2 - 54M^4a^2] + 24\sqrt{3}M^2\sqrt{(M^2 - a^2 - Q^2)[Q^2(9M^2 - 8Q^2)^2 - 27M^4a^2]}^3 \right\}^{\frac{1}{3}},$$

$$V = 3M^4a^2 + (M^2 - Q^2)[6(3M^2 - 2Q^2)^2 - 8Q^4]. \quad (45)$$

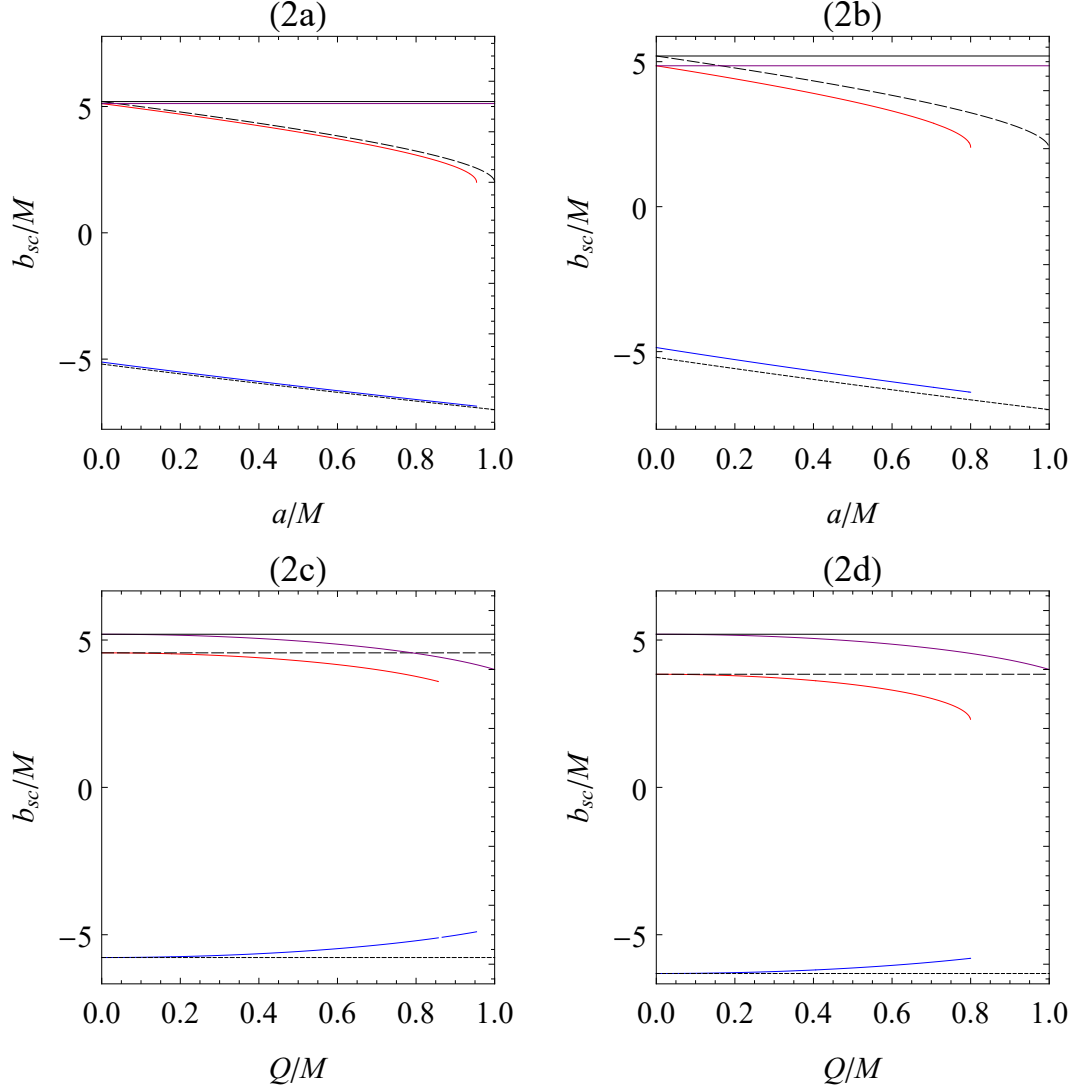


FIG. 2: The critical impact parameter b_{sc}/M as a function of the spin parameter a/M for (a) $Q/M = 0.3$, (b) $Q/M = 0.6$. Also, the critical impact parameter b_{sc}/M as a function of charge Q/M for (c) $a/M = 0.3$, (d) $a/M = 0.6$. The plots show the Schwarzschild, Reissner-Nordström, Kerr and Kerr-Newman black holes for comparison. The plot convention used henceforth: Kerr-Newman direct (solid red line), Kerr-Newman retrograde (solid blue line), Kerr direct (black dashed line with $Q = 0$), Kerr retrograde (black dotted line, with $Q = 0$), Reissner-Nordström (solid purple line, with $a = 0$), and Schwarzschild (solid black line, with $Q = 0, a = 0$).

These will serve as the important inputs for the analytical expressions of the coefficients \bar{a} and \bar{b} in (1).

The counterpart of (16) for the Kerr-Newman case as a function of z in (15) can be easily

derived giving

$$\frac{dz}{d\phi} = \frac{1}{r_0} \frac{1 - \frac{2M}{r_0}(1-z) + \frac{a^2+Q^2}{r_0^2}(1-z)^2}{1 - \frac{2M}{r_0}(1 - \frac{a}{b_s})(1-z) + \frac{Q^2}{r_0^2}(1 - \frac{a}{b_s})(1-z)^2} \sqrt{B(z, r_0)}, \quad (46)$$

where

$$B(z, r_0) = c_1(r_0)z + c_2(r_0)z^2 + c_3(r_0)z^3 + c_4(r_0)z^4. \quad (47)$$

The function $B(z, r_0)$ is then the quartic polynomial in z with the coefficients

$$\begin{aligned} c_1(r_0) &= 4Q^2 \left(1 - \frac{a}{b_s}\right)^2 - 6Mr_0 \left(1 - \frac{a}{b_s}\right)^2 + 2r_0^2 \left(1 - \frac{a^2}{b^2}\right), \\ c_2(r_0) &= -6Q^2 \left(1 - \frac{a}{b_s}\right)^2 + 6Mr_0 \left(1 - \frac{a}{b_s}\right)^2 - r_0^2 \left(1 - \frac{a^2}{b^2}\right), \\ c_3(r_0) &= 4Q^2 \left(1 - \frac{a}{b_s}\right)^2 - 2Mr_0 \left(1 - \frac{a}{b_s}\right)^2, \\ c_4(r_0) &= -Q^2 \left(1 - \frac{a}{b_s}\right)^2. \end{aligned} \quad (48)$$

All coefficients have the additional contributions from the charge Q . In particular, the presence of the z^4 term with the coefficient $c_4(r_0)$ in B , which vanishes in the Kerr case, makes the calculations of \bar{a} and \bar{b} more involved. The integrant function $f(z, r_0)$ in (22) now takes the form

$$f(z, r_0) = \frac{r_0^2}{a^2 + Q^2} \left(\frac{C_-}{z - z_-} + \frac{C_Q z + C_+}{z - z_+} \right) \frac{2r_0}{\sqrt{c_1(r_0)z + c_2(r_0)z^2 + c_3(r_0)z^3 + c_4(r_0)z^4}}. \quad (49)$$

The corresponding coefficients C_- , C_Q , and C_+ in the Kerr-Newman case are

$$\begin{aligned} C_- &= \frac{a^2 + Q^2 - 2Mr_-(1 - \frac{a}{b_s}) + \frac{Q^2 r_-^2}{a^2 + Q^2} (1 - \frac{a}{b_s})}{2r_0 \sqrt{M^2 - a^2 - Q^2}}, \\ C_Q &= \frac{Q^2}{r_0^2} \left(1 - \frac{a}{b_s}\right), \\ C_+ &= \frac{a^2 + Q^2 - 2Mr_-(1 - \frac{a}{b_s}) + \frac{Q^2}{r_0} (r_+ - r_-) (1 - \frac{a}{b_s}) + Q^2 (1 - \frac{a}{b_s})}{-2r_0 \sqrt{M^2 - a^2 - Q^2}}, \end{aligned} \quad (50)$$

where z_+ , z_- then become

$$\begin{aligned} z_- &= 1 - \frac{r_0 r_-}{a^2 + Q^2}, \\ z_+ &= 1 - \frac{r_0 r_+}{a^2 + Q^2}, \end{aligned} \quad (51)$$

defined in terms of the outer(inner) black hole horizon r_+ (r_-). Again, $z_{\pm} \leq 0$ for all a and Q with the nonzero r_+ . Note that, for charge $Q \rightarrow 0$, C_Q vanishes.

Analogous to the previous subsection of the Kerr case, we define the function $f_D(z, r_0)$ as

$$f_D(z, r_0) = \frac{r_0^2}{a^2 + Q^2} \left(\frac{C_-}{z - z_-} + \frac{C_Q z + C_+}{z - z_+} \right) \frac{2r_0}{\sqrt{c_1(r_0)z + c_2(r_0)z^2}}. \quad (52)$$

As $z \rightarrow 0$, $f_D(z, r_0) \rightarrow 1/z$. Its integration over z gives the divergent part of $I_D(r_0)$ when $b \rightarrow b_c$. Here we find

$$\begin{aligned} I_D(r_0) &= \int_0^1 f_D(z, r_0) dz \\ &= \frac{2r_0^3}{a^2 + Q^2} \frac{C_-}{\sqrt{c_1(r_0)z_- + c_2(r_0)z_-^2}} \log \left(\frac{\sqrt{c_1(r_0)z_- + c_2(r_0)z_-} + \sqrt{c_1(r_0) + c_2(r_0)z_-}}{\sqrt{c_1(r_0)z_- + c_2(r_0)z_-} - \sqrt{c_1(r_0) + c_2(r_0)z_-}} \right) \\ &\quad + \frac{2r_0^3}{a^2 + Q^2} \frac{C_+ + C_Q z_+}{\sqrt{c_1(r_0)z_+ + c_2(r_0)z_+^2}} \log \left(\frac{\sqrt{c_1(r_0)z_+ + c_2(r_0)z_+} + \sqrt{c_1(r_0) + c_2(r_0)z_+}}{\sqrt{c_1(r_0)z_+ + c_2(r_0)z_+} - \sqrt{c_1(r_0) + c_2(r_0)z_+}} \right) \\ &\quad - \frac{2r_0^3}{a^2 + Q^2} \frac{2C_Q}{\sqrt{c_2(r_0)}} \log \left(\sqrt{c_1(r_0)} \sqrt{c_2(r_0)} \right) \\ &\quad + \frac{2r_0^3}{a^2 + Q^2} \frac{2C_Q}{\sqrt{c_2(r_0)}} \log \left(c_2(r_0) + \sqrt{c_2(r_0)} \sqrt{c_1(r_0) + c_2(r_0)} \right). \end{aligned} \quad (53)$$

In the SDL, by substituting (29), $I_D(b)$ becomes

$$\begin{aligned} I_D(b) &\approx - \frac{r_{sc}^3}{a^2 + Q^2} \left(\frac{C_{-sc}}{\sqrt{c_{2sc}z_{-sc}^2}} + \frac{C_{+sc} + C_{Qsc}z_{+sc}}{\sqrt{c_{2sc}z_{+sc}^2}} + \frac{C_{Qsc}}{\sqrt{c_{2sc}}} \right) \log \left(\frac{b}{b_{sc}} - 1 \right) \\ &\quad + \frac{r_{sc}^3}{a^2 + Q^2} \frac{C_{-sc}}{\sqrt{c_{2sc}z_{-sc}^2}} \log \left[\frac{16c_{2sc}^2 z_{-sc}^2 b_{sc}''}{c_{1sc}^2 2b_{sc}(z_{-sc} - 1)^2} \right] \\ &\quad + \frac{r_{sc}^3}{a^2 + Q^2} \frac{C_{+sc} + C_{Qsc}z_{+sc}}{\sqrt{c_{2sc}z_{+sc}^2}} \log \left[\frac{16c_{2sc}^2 z_{+sc}^2 b_{sc}''}{c_{1sc}^2 2b_{sc}(z_{+sc} - 1)^2} \right] + \frac{r_{sc}^3}{a^2 + Q^2} \frac{C_{Qsc}}{\sqrt{c_{2sc}}} \log \left[\frac{16c_{2sc}^2 b_{sc}''}{c_{1sc}^2 2b_{sc}} \right], \end{aligned} \quad (54)$$

from which we can read off the coefficients \bar{a} and b_D as follows

$$\bar{a} = \frac{r_{sc}^3}{\sqrt{c_{2sc}}} \left[\frac{C_{-sc}}{r_{sc}r_- - (a^2 + Q^2)} + \frac{C_{+sc}}{r_{sc}r_+ - (a^2 + Q^2)} \right] \quad (55)$$

$$\begin{aligned} b_D &= \bar{a} \log \left[\frac{8c_{2sc}^2 b_{sc}''}{c_{1sc}^2 b_{sc}} \right] \\ &\quad + \frac{2r_{sc}^3}{\sqrt{c_{2sc}}} \left[\frac{C_{-sc}}{r_{sc}r_- - (a^2 + Q^2)} \log \left(1 - \frac{a^2 + Q^2}{r_{sc}r_-} \right) + \frac{C_{+sc} + C_{Qsc}z_{+sc}}{r_{sc}r_+ - (a^2 + Q^2)} \log \left(1 - \frac{a^2 + Q^2}{r_{sc}r_+} \right) \right]. \end{aligned} \quad (56)$$

They reduce to their counterparts in (31) and (32) respectively as $Q \rightarrow 0$. As for the remaining contributions to the regular part, and in the SDL, we have

$$\begin{aligned}
b_R &= I_R(r_{sc}) = \int_0^1 f_R(z, r_{sc}) dz \\
&= \frac{2r_0^3}{a^2 + Q^2} \frac{C_-}{\sqrt{c_2} z_-} \log \left(\frac{z_-}{z_- - 1} \frac{2c_2 + c_3 + 2\sqrt{c_2 + c_3 + c_4}\sqrt{c_2}}{4c_2} \right) \\
&+ \frac{2r_0^3}{a^2 + Q^2} \frac{C_-}{z_- \sqrt{c_2 + c_3 z_- + c_4 z_-^2}} \log \left(\frac{z_- - 1}{z_-} \frac{\left(\sqrt{c_2 + c_3 z_- + c_4 z_-^2} + \sqrt{c_2} \right)^2 - c_4 z_-^2}{\left(\sqrt{c_2 + c_3 z_- + c_4 z_-^2} + \sqrt{c_2 + c_3 + c_4} \right)^2 - c_4 (z_- - 1)^2} \right) \\
&+ \frac{2r_0^3}{a^2 + Q^2} \frac{C_+}{\sqrt{c_2} z_+} \log \left(\frac{z_+}{z_+ - 1} \frac{2c_2 + c_3 + 2\sqrt{c_2 + c_3 + c_4}\sqrt{c_2}}{4c_2} \right) \\
&+ \frac{2r_0^3}{a^2 + Q^2} \frac{C_+ + C_Q z_+}{z_+ \sqrt{c_2 + c_3 z_+ + c_4 z_+^2}} \log \left(\frac{z_+ - 1}{z_+} \frac{\left(\sqrt{c_2 + c_3 z_+ + c_4 z_+^2} + \sqrt{c_2} \right)^2 - c_4 z_+^2}{\left(\sqrt{c_2 + c_3 z_+ + c_4 z_+^2} + \sqrt{c_2 + c_3 + c_4} \right)^2 - c_4 (z_+ - 1)^2} \right) \\
&+ \frac{2r_0^3}{a^2 + Q^2} \frac{C_Q}{\sqrt{c_2}} \log \left(\frac{z_+}{z_+ - 1} \right) \Big|_{r_0=r_{sc}}
\end{aligned} \tag{57}$$

In the limit of $Q \rightarrow 0$, where C_Q and c_4 go to zero, the above expression of b_R reduces to (33) in the Kerr case after implementing straightforward algebra. The coefficient \bar{b} is obtained using (56) and (57) as

$$\begin{aligned}
\bar{b} &= -\pi + \bar{a} \log \left[\frac{36}{4(1 - c_{4sc}/c_{2sc})^2 + 4\sqrt{3}(1 - c_{4sc}/c_{2sc})^{3/2} + 3(1 - c_{4sc}/c_{2sc})} \frac{8c_{2sc}^2 b_{sc}''}{c_{1sc}'^2 b_{sc}} \right] \\
&+ \frac{r_{sc}^3}{\sqrt{c_{2sc}}} \frac{2(a^2 + Q^2)C_{-sc}}{(a^2 + Q^2 - r_{sc}r_-)} \frac{\sqrt{3}}{P_-} \\
&\times \log \left[\frac{-r_{sc}r_-}{a^2 + Q^2 - r_{sc}r_-} \frac{(P_- + \sqrt{3}(a^2 + Q^2))^2 - 3(a^2 + Q^2 - r_{sc}r_-)^2 (c_{4sc}/c_{2sc})}{(P_- + (a^2 + Q^2)(1 - c_{4sc}/c_{2sc})^{1/2})^2 - 3r_{sc}^2 r_-^2 (c_{4sc}/c_{2sc})} \right] \\
&+ \frac{r_{sc}^3}{\sqrt{c_{2sc}}} \frac{2[(a^2 + Q^2)C_{+sc} + (a^2 + Q^2 - r_{sc}r_+)C_{Qsc}]}{(a^2 + Q^2 - r_{sc}r_+)} \frac{\sqrt{3}}{P_+} \\
&\times \log \left[\frac{-r_{sc}r_+}{a^2 + Q^2 - r_{sc}r_+} \frac{(P_+ + \sqrt{3}(a^2 + Q^2))^2 - 3(a^2 + Q^2 - r_{sc}r_+)^2 (c_{4sc}/c_{2sc})}{(P_+ + (a^2 + Q^2)(1 - c_{4sc}/c_{2sc})^{1/2})^2 - 3r_{sc}^2 r_+^2 (c_{4sc}/c_{2sc})} \right].
\end{aligned} \tag{58}$$

In the equation above, we have replaced c_{3sc} by the linear combination of c_{2sc} and c_{4sc} in (48), given by

$$c_{3sc} = -\frac{2}{3}c_{2sc} - \frac{4}{3}c_{4sc}. \tag{59}$$

We also have

$$P_{\pm}^2 = (a^2 + Q^2 + 2r_{sc}r_{\pm})(a^2 + Q^2) - (a^2 + Q^2 + r_{sc}r_{\pm})(a^2 + Q^2 - r_{sc}r_{\pm})(c_{4sc}/c_{2sc}). \quad (60)$$

Combining (41), (42) and (44), the coefficients \bar{a} and \bar{b} in (55) and (58) can be analytically expressed as a function of the black hole's parameters in the SDL. Our results are plotted in Fig.(4). Again, notice that $\bar{a} > 0$ but $\bar{b} < 0$ with the parameters in the figure. Due to the fact that the bending angle for light rays resulting from the charged black hole is suppressed as compared with the neutral black hole with the same impact parameter b , both \bar{a} and $|\bar{b}|$ are found to increase with the charge Q .

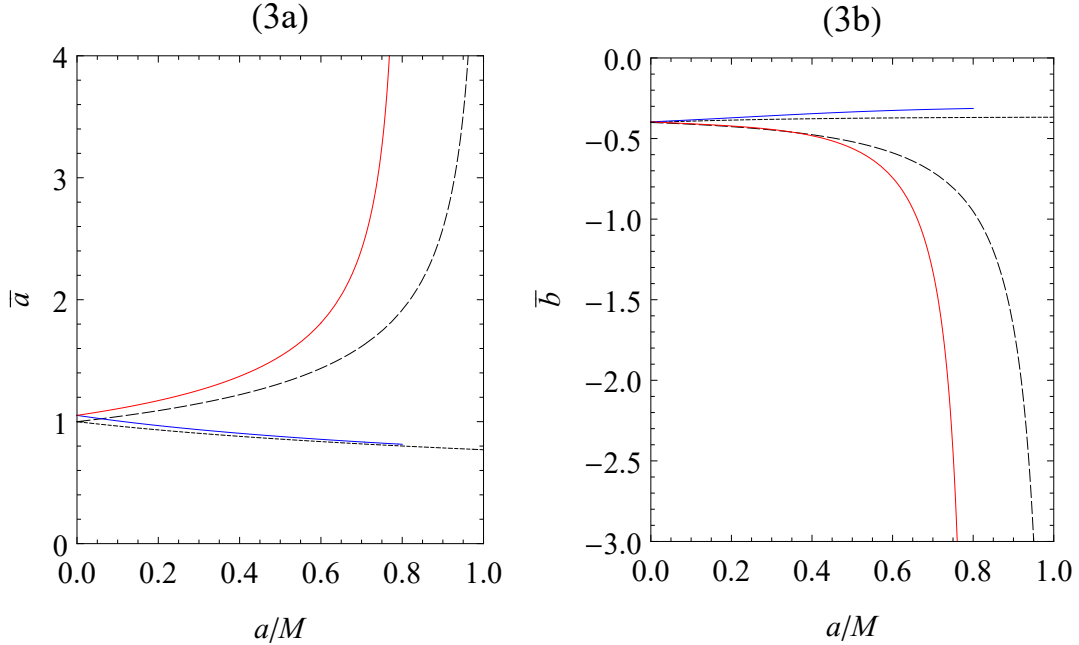


FIG. 3: The coefficients \bar{a} and \bar{b} as a function of the spin parameter a/M for the Kerr black hole with $Q/M = 0$ and the Kerr-Newman black hole with $Q/M = 0.6$: (a) the coefficient \bar{a} , (b) the coefficient \bar{b} . The display of the plot follows the convention in Fig.(2).

It is then quite straightforward to check that the coefficients \bar{a} and \bar{b} in the Kerr-Newmann case can reduce to those in (31) and (35) in the Kerr case by setting $c_4 \rightarrow 0$ in the limit of $Q \rightarrow 0$, also leading to $P_{\pm} \rightarrow a\sqrt{a^2 + 2r_{sc}r_{\pm}}$. To compare with the Reissner-Nordström black hole in [12, 13], it is known that the impact parameter b as a function of r_0 is

$$b(r_0) = \frac{r_0^2}{\sqrt{Q^2 - 2Mr_0 + r_0^2}} \quad (61)$$

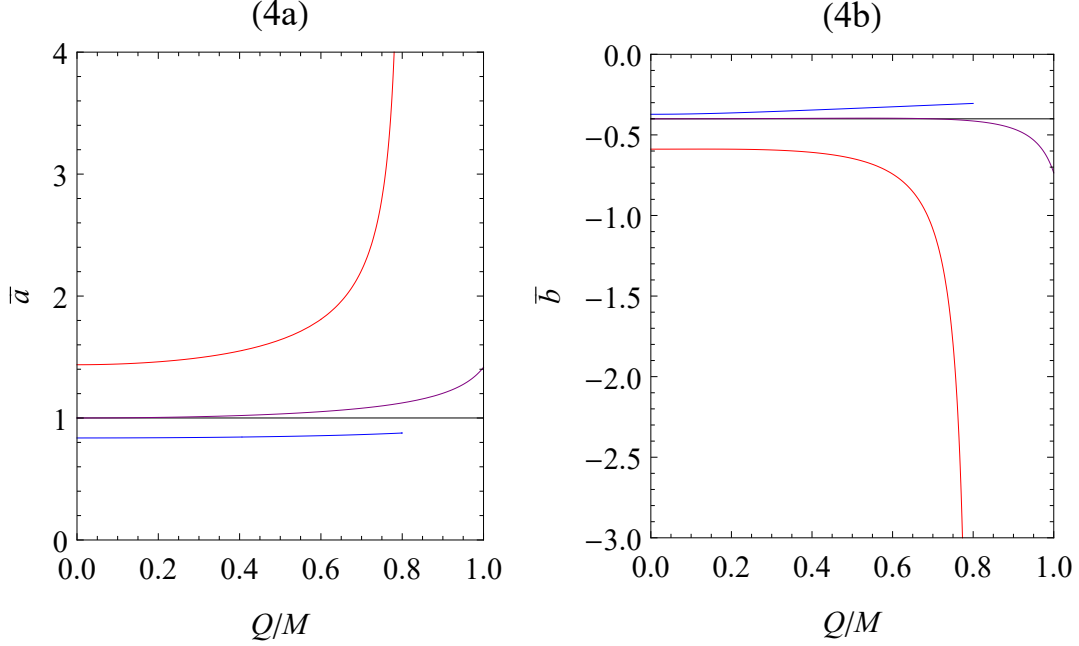


FIG. 4: The coefficients of \bar{a} and \bar{b} as a function of charge Q/M for the Schwarzschild black hole with $a/M = 0$, $Q/M = 0$, the the Reissner-Nordström blk hole with $a/M = 0$ and the Kerr-Newman black hole with $a/M = 0.6$: (a) the coefficient \bar{a} , (b) the coefficient \bar{b} . The display of the plot follows the convention in Fig.(2).

and the circular motion of light rays forms the photon sphere with the radius

$$r_c = \frac{3M + \sqrt{9M^2 - 8Q^2}}{2}. \quad (62)$$

The critical impact parameter as a function of r_c is given by

$$b_c = \frac{r_c^2}{\sqrt{Mr_c - Q^2}}. \quad (63)$$

Notice the subscript is changed from sc to c since the same critical impact parameters are obtained for light rays in direct orbits and retrograde orbits in the case of the nonspinning black holes. In the limit of $a \rightarrow 0$, we have $C_{-sc} \rightarrow 0$ in (50) using the definition of r_- in (39). Thus, the coefficient \bar{a} in (55) can be further simplified using (50), (39) and $c_{1sc} = 0$ giving

$$\bar{a} = \frac{r_c}{\sqrt{3Mr_c - 4Q^2}}, \quad (64)$$

which reproduces the expression in [12, 13]. As for the coefficient \bar{b} , in the limit of $a \rightarrow 0$, apart from $C_{-sc} \rightarrow 0$, $(a^2 + Q^2)C_{+sc} + (a^2 + Q^2 - r_{sc}r_+)C_{Qsc} \rightarrow 0$ as well. So, the coefficient

\bar{b} in (58) has the contribution only from the term proportional to \bar{a} . After substituting (61) and (48) in the limit of $a \rightarrow 0$ to (58) and going through nontrivial algebra, we indeed recover the compact analytical expression in [12, 13]:

$$\bar{b} = -\pi + \bar{a} \log \left[\frac{8(3Mr_c - 4Q^2)^3}{M^2 r_c^2 (Mr_c - Q^2)^2} \left(2\sqrt{Mr_c - Q^2} - \sqrt{3Mr_c - 4Q^2} \right)^2 \right]. \quad (65)$$

Figure 5 shows good agreement between the obtained SDL expression and the exact one in [23] computed numerically when b approaches b_c for some values of a and Q .

In conclusion, we have successfully achieved the analytical expression of the coefficient \bar{a} and \bar{b} in the form (1) of the SDL deflection angle due to the spherically nonsymmetric black holes, although they look not as simple as in the cases of the spherically symmetric black holes. Additionally, the obtained expressions can reproduce the respective ones due to the Kerr, Reissner-Nordström black holes and also due to the Schwarzschild black hole by taking the appropriate limits of the black hole's parameters.

III. RELATIVISTIC IMAGES OF GRAVITATIONAL LENS AND APPLICATIONS TO SUPERMASSIVE GALACTIC BLACK HOLES

We consider the cases of the planar light rays with the lens diagram shown in Fig.(1), where d_L and d_S are the distances of the lens (black hole) and the light source from the observer, and also d_{LS} represents the distance between the lens and the source. The line joining the observer and the lens is considered as a reference optical axis. The angular positions of the source and the image are measured from the optical axis, and are denoted by β and θ , respectively. The lens equation is given by

$$\tan s\beta = \tan \theta - \frac{d_{LS}}{d_S} [\tan \theta + \tan(\hat{\alpha} - \theta)], \quad (66)$$

where $\hat{\alpha}$ is the deflection angle of light rays obtained from (22) that can be expressed in terms of the impact parameter b as the light rays approach to the black holes. In [10], it is mentioned that the lens equations are applied for the observer and the source immersed in the asymptotically flat spacetime, where the Kerr and Kerr-Newman black holes have the asymptotically flat metric. Also, in the small β and θ limits, we will see that the approximate lens equations to be found later are the same ones in [8], in which the Kerr black holes are considered. In the SDL of our interest, when the light rays wind around the black hole n

times, the deflection angle $\hat{\alpha}$ can be approximately by (1). The angle appearing in the lens equation should be within 2π and can be obtained from the deflection angle $\hat{\alpha}$ subtracting $2n\pi$.

Together with the relation between the impact parameter b and the angular position of the image given by

$$b = d_L \sin \theta, \quad (67)$$

in Fig.(1), we can solve the lens equation (66) with a given angular position of the source β for the angular position of the observed image θ . In the SDL, when the angular position of the source is small, θ is expectedly small with the small impact parameter b . Then the lens equation (66) can be further simplified by

$$s\beta \simeq \theta - \frac{d_{LS}}{d_S} [\hat{\alpha}(\theta) - 2n\pi] \quad (68)$$

and (67) can be approximated by $b \simeq d_L \theta$. This can reduce to the lens equations in [8], in which the small angle limits are considered. According to [9], the zeroth order solution θ_{sn}^0 is obtained from $\hat{\alpha}(\theta_{sn}^0) = 2n\pi$. Using the SDL deflection angle in (1) we have then

$$\theta_{sn}^0 = \frac{|b_{sc}|}{d_L} \left(1 + e^{\frac{\bar{b}-2n\pi}{\bar{a}}} \right) \quad (69)$$

for $n = 1, 2, \dots$. The angular position θ_{sn} decrease in n and reaches the asymptotic angular position given by $\theta_{s\infty} = |b_{sc}|/d_L$ as $n \rightarrow \infty$. With the zeroth order solution (69), the expansion of $\hat{\alpha}(\theta)$ around $\theta = \theta_{sn}^0$ is written explicitly as

$$\hat{\alpha}(\theta) = \hat{\alpha}(\theta_{sn}^0) - \frac{\bar{a}}{e^{(\bar{b}-2n\pi)/\bar{a}}} \frac{d_L d_{LS}}{|b_{sc}| d_S} (\theta - \theta_{sn}^0) + O(\theta - \theta_{sn}^0)^2. \quad (70)$$

Then the approximate lens equation (68) to the order $(\theta - \theta_{sn}^0)$ becomes

$$s\beta \simeq \theta_{sn}^0 + \left(1 + \frac{\bar{a}}{e^{(\bar{b}-2n\pi)/\bar{a}}} \frac{d_L d_{LS}}{|b_{sc}| d_S} \right) (\theta - \theta_{sn}^0). \quad (71)$$

Solving for θ , by keeping the lowest order term in $|b_{sc}|/d_L \ll 1$, we find the angular position of the image as [7]

$$\theta_{sn} \simeq \theta_{sn}^0 + \frac{e^{(\bar{b}-2n\pi)/\bar{a}}}{\bar{a}} \frac{|b_{sc}| d_S}{d_L d_{LS}} (s\beta - \theta_{sn}^0). \quad (72)$$

We assume that either Kerr or Kerr-Newman black holes have the clockwise rotation shown in Fig.(1). The light rays emitted from the source circle around the black hole

multiple times in the SDL along a direct orbit (red line) with $s = +1$, where both the image and the source end up in the same sides of the optical axis with the angular position θ_{+n} and/or along a retrograde orbit (blue line) with $s = -1$, where the image and the source are in the opposite sides with the angular position θ_{-n} . We also define the angular position difference between the outermost image $\theta_{1\pm}$ and the asymptotic one near the optical axis as

$$\Delta\theta_s = \theta_{s1} - \theta_{s\infty} , \quad (73)$$

which is the value to compare with the resolution of the observation that allows to distinguish among a set of the relativistic images.

We now compute the angular positions of the relativistic images of the sources for $n = 1$ (the outermost image) due to either Kerr or Kerr-Newman black holes with the mass $M = 4.1 \times 10^6 M_\odot$ and the distance $d_L = 26000$ ly of the supermassive black hole Sagittarius A* at the center of our Galaxy as an example. We also take the ratio to be $d_{LS}/d_S = 1/2$. In Table 1 (2), we consider both the image and the source are in the same (opposite) sides of the optical axis, where the light rays travel along the direct (retrograde) orbits, and choose $\beta \sim \theta_{\pm 1}$. The angular positions of the relativistic images are computed by (72). In the case of $|b_{sc}| \ll d_L$, θ_{sn} is not sensitive to β but mainly determined by θ_{sn}^0 in (69). Given \bar{a} and $|\bar{b}|$ of the magnitudes shown in Fig.(3) and (4), $e^{-\frac{|\bar{b}|+2n\pi}{\bar{a}}} \ll 1$. The behavior of θ_{sn} thus depends mainly on $|b_{sc}|$ as a function of angular momentum a and charge Q of the black holes.

As discussed in the previous section, since the effects from the angular momentum of the black hole for direct orbits effectively induces more repulsive effects compared with the retrograde orbits, clearly shown in their effective potential W_{eff} (9), the resulting $b_{+c} < |b_{-c}|$ yields asymmetric values of $\theta_{+1} < \theta_{-1}$ for the same a and Q . These features are shown in the Tables 1 and 2. Additionally, we notice that θ_{+1} (θ_{-1}) decreases (increases) in a for fixed Q resulting from the decrease (increase) of b_{+c} ($|b_{-c}|$) as a increases. As for $\Delta\theta$, for the same Q , $\Delta\theta_+$ increases with a whereas $\Delta\theta_-$ decreases with a . In particular, $\Delta\theta_+$ can be increased from about $10^{-2}\mu\text{as}$ with $a/M \sim 10^{-3}$ and $Q/M = 10^{-3}$ to the value as high as $0.6\mu\text{as}$ with $a/M = 0.9$ and $Q/M = 10^{-3}$, which certainly increases their observability by the current very long baseline interferometry (VLBI) [29, 30]. As for the finite Q effects, also showing the repulsion to the light rays seen in the effective potential (40), both θ_{+1} and θ_{-1} decrease in Q for fixed a , resulting in the slightly increase of $\Delta\theta_{\pm}$ as Q increases.

Another application of the analytical expression of the deflection angle on the equatorial

a/M	Q/M	θ_{+1} (μas)	$\hat{\alpha}$	b/M	$\theta_{+\infty}$ (μas)	$\Delta\theta_+$ (μas)
10^{-3}	10^{-3}	26.4231	$2\pi + 32.8135$ (μas)	5.2007	26.3900	0.0331
	0.3	26.0217	$2\pi + 32.0563$ (μas)	5.1217	25.9866	0.0351
	0.6	24.7179	$2\pi + 29.4336$ (μas)	4.8651	24.6747	0.0432
	0.8	23.1445	$2\pi + 26.2837$ (μas)	4.5554	23.0849	0.0596
0.5	10^{-3}	20.9290	$2\pi + 21.8561$ (μas)	4.1193	20.8119	0.1171
	0.3	20.4085	$2\pi + 20.8203$ (μas)	4.0169	20.2758	0.1327
	0.6	18.6189	$2\pi + 17.2398$ (μas)	3.6646	18.4049	0.2140
	0.8	16.0922	$2\pi + 12.1835$ (μas)	3.1673	15.5372	0.5550
0.9	10^{-3}	15.1170	$2\pi + 10.2354$ (μas)	2.9754	14.4517	0.6653
	0.3	14.1818	$2\pi + 8.36638$ (μas)	2.7913	13.2701	0.9117
	0.6
	0.8

TABLE I: Relativistic images on the same side of the source with the angular position $\beta = 10$ (μas) where the light rays are along direct orbits seen in Fig.(1).

plane is to consider the quasiequatorial gravitational lensing based upon the works of [8, 31]. In this situation, the polar angle θ is set to be slightly away from $\theta = \frac{\pi}{2}$ and now becomes time dependent. In the SDL, the deflection angle of light rays with the additional initial declination can also be cast into the form of (1) where the coefficients are replaced by \hat{a} and \hat{b} . In particular, the coefficient \hat{a} obtained from the slightly off the equatorial plane can be related by the coefficient \bar{a} on the equatorial plane through the ω function as

$$\hat{a} = \omega(r_{sc}) \bar{a} , \quad (74)$$

where ω depends on r , and in turn depends on the deflection angle $\phi(r)$. Notice that the above relation (74) involves ω , which is evaluated at $r = r_{sc}$. In the case of the Kerr black hole, it is found that [8]

$$\omega(r_{sc}) = \frac{(r_{sc}^2 + a^2 - 2Mr_{sc})\sqrt{b_{sc}^2 - a^2}}{2Mar_{sc} + b_{sc}(r_{sc}^2 - 2Mr_{sc})} , \quad (75)$$

and thus for the Schwarzschild case we have $a \rightarrow 0$, $\omega \rightarrow 1$. Then, substituting (13) and (14) into (75), together with the expression of \bar{a} in (31), through (74) gives $\hat{a} = 1$ for the Kerr

a/M	Q/M	θ_{-1} (μas)	$\hat{\alpha}$	b/M	$\theta_{-\infty}$ (μas)	$\Delta\theta_-$ (μas)
10^{-3}	10^{-3}	26.4433	$2\pi + 72.8286$ (μas)	5.20464	26.4103	0.0330
	0.3	26.0422	$2\pi + 72.0654$ (μas)	5.12569	26.0073	0.0349
	0.6	24.7395	$2\pi + 69.4844$ (μas)	4.86931	24.6966	0.0429
	0.8	23.1680	$2\pi + 66.3165$ (μas)	4.56000	23.1088	0.0592
0.5	10^{-3}	31.1994	$2\pi + 82.4458$ (μas)	6.14075	31.1862	0.0132
	0.3	30.8561	$2\pi + 81.6482$ (μas)	6.07318	30.8422	0.0139
	0.6	29.7638	$2\pi + 79.5352$ (μas)	5.85820	29.7479	0.0159
	0.8	28.5058	$2\pi + 76.9916$ (μas)	5.61059	28.4866	0.0192
0.9	10^{-3}	34.7203	$2\pi + 89.4397$ (μas)	6.83374	34.7130	0.0073
	0.3	34.4063	$2\pi + 88.5984$ (μas)	6.77195	34.3988	0.0075
	0.6
	0.8

TABLE II: Relativistic images on the opposite side of the source with the angular position $\beta = 10$ (μas) where the light rays are in retrograde orbits seen in Fig.(1).

case. However, in the Kerr-Newman black hole, the straightforward calculations show that the above relation (74) still holds true. The detailed derivations will appear in our future publication. Thus, the coefficient \hat{a} can be analytically given by the coefficient \bar{a} in (55), together with the ω function in the Kerr-Newman case in below

$$\omega(r_{sc}) = \frac{(r_{sc}^2 + a^2 + Q^2 - 2Mr_{sc})\sqrt{b_{sc}^2 - a^2}}{-a(Q^2 - 2Mr_{sc}) + b_{sc}(r_{sc}^2 + Q^2 - 2Mr_{sc})}. \quad (76)$$

As $Q \rightarrow 0$, (76) reduces to (75) in the Kerr case. The behavior of \hat{a} as a function of the charge Q with the choices of the angular momentum a for direct and retrograde orbits is displayed in Fig.(6). The value of \hat{a} ($\hat{a} > 1$) increases with Q for both direct and retrograde orbits. According to [8, 31], the magnification of relativistic images might formally diverge when the angular positions of the sources are at caustic points. The corresponding magnifying power close to caustic points due to the light rays winding around the black hole n times is given by $\bar{\mu}_n$ with the ratio between two neighboring caustic points

$$\frac{\bar{\mu}_{n+1}}{\bar{\mu}_n} \propto e^{-\pi/\hat{a}} \quad (77)$$

depending only on \hat{a} . In the Kerr case with $\hat{a} = 1$, this ratio is independent of the black hole angular momentum a , whereas in the Kerr-Newman case with $\hat{a} > 1$ shown in the Fig.(6), the ratio decreases with Q for both direct and retrograde orbits [31]. Here we just sketch some of the effects from the charge Q of the black hole on the magnification of relativistic images. To have the full pictures of the caustic points and find the magnification of relativistic images, it in fact deserves the extensive study to compute not only \hat{a} but also \hat{b} by following [8, 31]. The further extension from quasiequatorial plane to the full sky is also of great interest [30, 32, 33].

IV. SUMMARY AND OUTLOOK

In summary, the dynamics of light rays traveling around the Kerr black hole and the Kerr-Newman black hole, respectively, is studied with the detailed derivations on achieving analytical expressions of \bar{a} and \bar{b} in the approximate form of the deflection angle in the SDL. Various known results are checked by taking the proper limits of the black hole's parameters. The analytical expressions are then applied to compute the angular positions of relativistic images due to the supermassive galactic black holes. We find that the effects from the angular momentum a for direct orbits of light rays and the charge Q for both direct and retrograde orbits increase the angular separation of the outermost images from the others. Although the observation of relativistic images is a very difficult task [29], our studies show potentially increasing observability of the relativistic images from the effects of angular momentum and charge of the black holes. Hopefully, relativistic images will be observed in the near future. Through the analytical results we present in this work, one can reconstruct the black hole's parameters that give strong lensing effects. As light rays travel on the quasiequatorial plane, our analytical results on the equatorial plane can also be applied to roughly estimate the relative magnifications of relativistic images with the sources near one of the caustic points by taking account of the dynamics of the light rays in the polar angle. The work of investigating the structure of the caustic points from the effects of the charge Q of the Kerr-Newman black holes and the magnification of relativistic images is in progress. Also, inspired by the recent advent of horizon-scale observations of astrophysical black holes, the properties of null geodesics become of great relevance to astronomy. The recent work of [30, 32, 33] provides an extensive analysis on Kerr black holes. We also plan

to extend the analysis of null geodesic to Kerr-Newman black holes, focusing on the effects from the charge of black holes.

Acknowledgments

This work was supported in part by the Ministry of Science and Technology, Taiwan, under Grant No.109-2112-M-259-003.

-
- [1] C. W. Misner, K. S. Thorne, and J. A. Wheeler, *Gravitation* (W. H. Freeman and Company, San Francisco, 1973).
 - [2] J. B. Hartle, *Gravity: An Introduction to Einstein's General Relativity* (Addison-Wesley, Reading, MA. 2003).
 - [3] P. Schneider, J. Ehlers, and E. E. Falco, *Gravitational Lenses* (Springer-Verlag, New York, Berlin, Heidelberg, 1992).
 - [4] K. S. Virbhadra and G. F. R. Ellis, Schwarzschild black hole lensing, *Phys. Rev. D* 62, 084003 (2000).
 - [5] S. Frittelli, T. P. Kling, and E. T. Newman, Spacetime perspective of Schwarzschild lensing, *Phys. Rev. D* 61, 064021 (2000).
 - [6] V. Bozza, S. Capozziello, G. Iovane, and G. Scarptta, Strong field limit of black hole gravitational lensing, *Gen. Relativ. Gravit.* 33, 1535 (2001).
 - [7] V. Bozza, Gravitational lensing in the strong field limit, *Phys. Rev. D* 66, 103001 (2002).
 - [8] V. Bozza, Quasiequatorial gravitational lensing by spinning black holes in the strong field limit, *Phys. Rev. D* 67, 103006 (2003).
 - [9] V. Bozza, Gravitational lensing by black holes, *Gen. Relativ. Gravit.* 42, 2269 (2010).
 - [10] E. F. Eiroa, G. E. Romero, and D. F. Torres, Reissner-Nordstrom black hole lensing, *Phys. Rev. D* 66, 024010 (2002).
 - [11] S. V. Iyer and A. O. Petters, Light's bending angle due to black holes: From the photon sphere to infinity, *Gen. Relativ. Gravit.* 39, 1563 (2007).
 - [12] N. Tsukamoto, Deflection angle in the strong deflection limit in a general asymptotically flat, static, spherically symmetric space-time, *Phys. Rev. D* 95, 064035 (2017).

- [13] N. Tsukamoto and Y. Gong, Retrolensing by a charged black hole, *Phys. Rev. D* 95, 064034 (2017).
- [14] K. S. Virbhadra and C. R. Keeton, Time delay and magnification centroid due to gravitational lensing by black holes and naked singularities, *Phys. Rev. D* 77, 124014 (2008).
- [15] R. Shaikh, P. Banerjee, S. Paul, and T. Sarkar, Strong gravitational lensing by wormholes, *J. Cosmol. Astropart. Phys.* 07, 028 (2019).
- [16] D. Richstone et al., Supermassive black holes and the evolution of galaxies, *Nature (London)* 14, 395 (1998).
- [17] A. Ghez, et al., High proper-motion stars in the vicinity of Sagittarius A*: Evidence for a supermassive black hole at the center of our galaxy, *Astrophys. J.* 509, 678 (1998).
- [18] R. Schodel, et al. A star in a 15.2-year orbit around the black hole at the centre of the Milky Way, *Nature (London)* 419, 694 (2002).
- [19] K. Akiyama et al., Event Horizon Telescope Collaboration, First M87 event horizon telescope results. I. The shadow of the supermassive black hole, *Astrophys. J.* 875, L1 (2019).
- [20] K. Akiyama et al., Event Horizon Telescope Collaboration, First M87 event horizon telescope results. V. Physical origin of the asymmetric ring, *Astrophys. J.* 875, L5 (2019).
- [21] K. Akiyama et al., Event horizon telescope collaboration, First M87 event horizon telescope results. VI. The shadow and mass of the central black hole, *Astrophys. J.* 875, L6 (2019).
- [22] S. V. Iyer and E. C. Hansen, Light's bending angle in the equatorial plane of a Kerr black hole, *Phys. Rev. D* 80, 124023 (2009).
- [23] Y.-W. Hsiao, D.-S. Lee, and C.-Y. Lin, Equatorial light bending around Kerr-Newman black holes, *Phys. Rev. D* 101, 064070 (2020).
- [24] J. R. Wilson, Some magnetic effects in stellar collapse and accretion, *Ann. N.Y. Acad. Sci.* 262, 123 (1975).
- [25] T. Damour, R. Hanni, R. Ruffini, and J. Wilson, Regions of magnetic support of a plasma around a black hole, *Phys. Rev. D* 17, 1518 (1978).
- [26] C.-Y. Liu, D.-S. Lee, and C.-Y. Lin, Geodesic motion of neutral particles around a Kerr-Newman black hole, *Classical Quantum Gravity* **34**, 235008 (2017).
- [27] C. Jiang and W. Lin, Post-Newtonian light propagation in Kerr-Newman spacetime, *Phys. Rev. D* 97, 024045 (2018).
- [28] G. V. Kraniotis, Gravitational lensing and frame dragging of light in the Kerr-Newman and

- the Kerr-Newman (anti) de Sitter black hole spacetimes, *Gen. Relativ. Gravit.* **46**, 1818 (2014).
- [29] J. S. Ulvestad, Goals of the ARISE Space VLBI Mission, *New Astron.Rev.* **43**, 531 (1999).
 - [30] M. D. Johnson, et al. Universal interferometric signatures of a black hole's photon ring, *Sci. Adv.* **6**, eaaz1310 (2020).
 - [31] G. N. Gyulchev and S. S. Yazadjiev, Kerr-Sen dilaton-axion black hole lensing in the strong deflection limit, *Phys. Rev. D* **75**, 023006 (2007).
 - [32] S. E. Gralla and A. Lupsasca, Null geodesics of the Kerr exterior, *Phys. Rev. D* **101**, 044032 (2020).
 - [33] S. E. Gralla and A. Lupsasca, Lensing by Kerr black holes, *Phys. Rev. D* **101**, 044031 (2020).

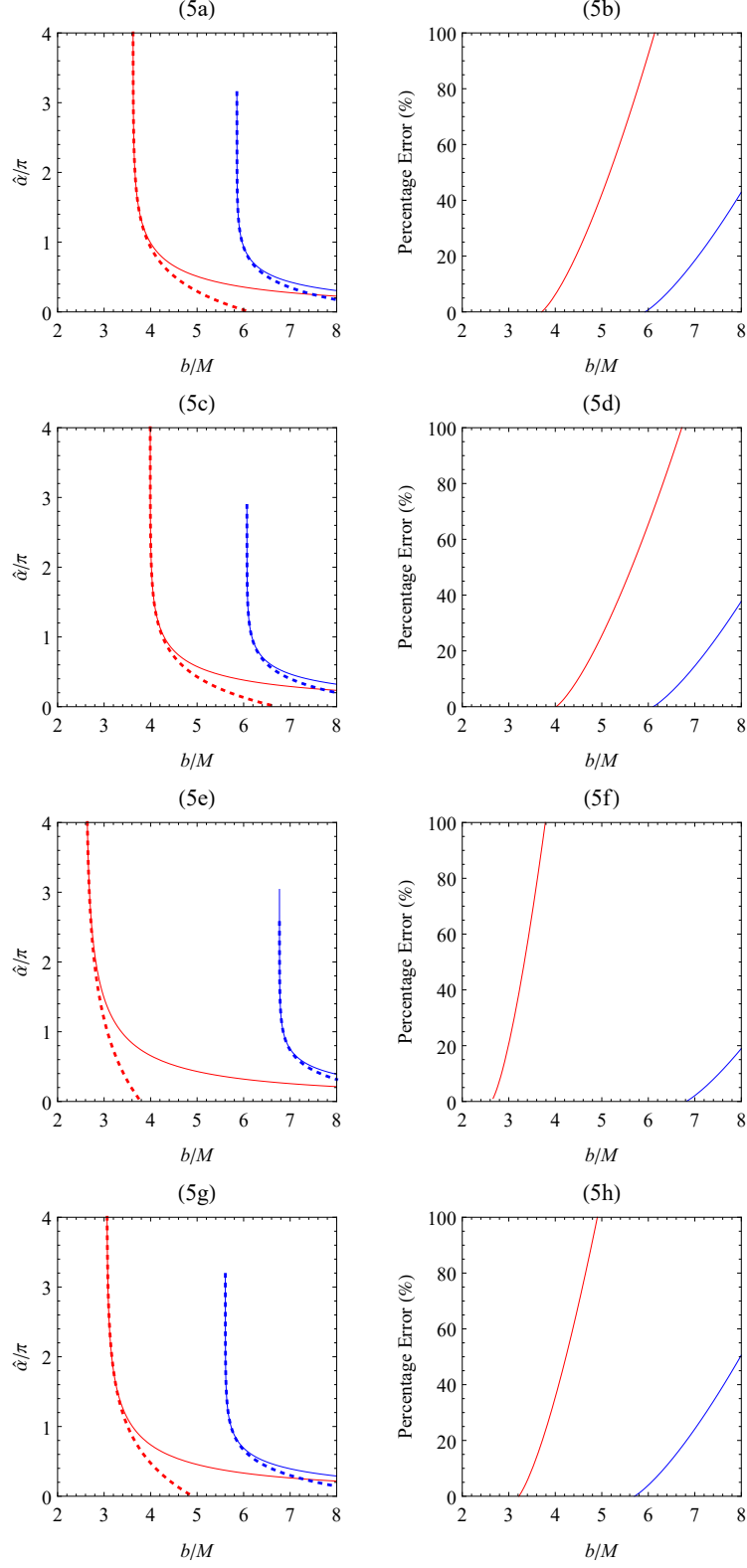


FIG. 5: The SDL deflection angle (dotted lines) and the exact one (solid lines): (a) $a/M = 0.5$ and $Q/M = 0.6$, (b) Error between them defined by $(\hat{\alpha}_{exact} - \hat{\alpha})/\hat{\alpha}_{exact} \times 100\%$; (c) $a/M = 0.5$ and $Q/M = 0.3$, (d) Error; (e) $a/M = 0.9$ and $Q/M = 0.3$, (f) Error; (g) $a/M = 0.5$ and $Q/M = 0.8$, (h) Error.

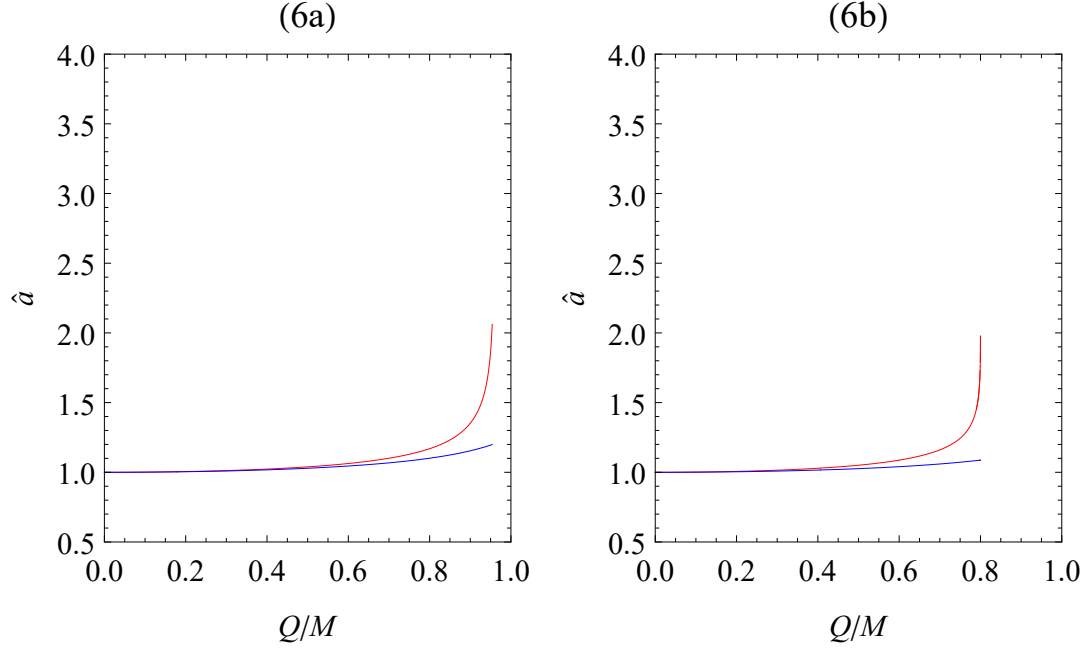


FIG. 6: The coefficient \hat{a} as a function of the black hole charge Q/M for the direct (retrograde) orbits with (a) $a/M = 0.3$, (b) $a/M = 0.6$. The display of the plot follows the convention in Fig.(2).